

SIMULATION DIAGNOSTICS OF MULTIPLE **DISCONTINUITIES** IN A MICROWAVE COAXIAL TRANSMISSION LINE*

Tom Y. Otoshi†

ABSTRACT

Multiple **discontinuities** in microwave transmission lines can cause unusual reflection and transmission loss characteristics as functions of frequency. This article presents a method for developing models that simulate return loss and insertion loss data measured over a broad band of frequencies. The overall cable is modeled as one consisting of shunt susceptance **discontinuities** separated by line lengths. A nonlinear least-squares fit is then performed between theoretical data (from the model) and experimental data. When this method was applied to modeling **discontinuities** in a slightly damaged S-band antenna cable, excellent agreement between theory and experiment was obtained over a frequency range of 1.70–2.85 GHz. The probable causes of the **discontinuities** are described. The same technique can be used for simulations and diagnostics of **discontinuities** in other types of microwave transmission lines such as rectangular and circular waveguides.

10 INTRODUCTION

The Galileo spacecraft, launched on October 18, 1989, is currently on its interplanetary journey to encounter Jupiter in 1995. Prior to launch, Galileo underwent environmental testing in the Space Simulator at the Jet Propulsion Laboratory (JPL). After these tests, it was discovered that the S-band output power had dropped about 0.2 dB at the transmit frequency of 2.295 GHz.

*The research **described** in this publication was carried out by the Jet Propulsion Laboratory, California Institute of Technology, under a contract with the National Aeronautics and Space Administration.

†The author is with the Jet Propulsion Laboratory, California Institute of Technology, Pasadena, California 91109.

More alarming were the radical changes observed in the insertion loss characteristics of the S-band antenna cable. Instead of the small peak-to-peak sinusoidal variations seen on pre-environmental test data, numerous nonperiodic humps and valleys (of unusual amplitudes) were seen on the post-environmental data over a frequency range of 1.7–2.85 GHz.

A task was undertaken to determine the cause of the radical changes, In the following, Section II presents the methodology used to develop models of the antenna cable, which was suspected of having been damaged by environmental testing. Section III presents results of models obtained with and without the aid of a nonlinear least-squares fit (NLSF) program. It is shown that the final model, obtained with the NLSF program, provided theoretical data that gave excellent agreement with all available experimental data over the entire frequency range.

H. METHODOLOGY

A. GENERAL PROCEDURE

The first step in the modeling procedure, used to obtain the results of this article, was to measure S-parameters of the suspected-damaged cable over a frequency range centered at the particular frequency of interest. From the measured S-parameter data, return-loss time domain plots were generated showing the approximate locations of discontinuities in the cable. The return-loss magnitude information on the time domain plots was used to synthesize equivalent circuit elements of individual discontinuities (see Appendix A). Then the overall cable was modeled as one consisting of individual shunt susceptances (representing discontinuities) separated by different lengths of lossy coaxial line sections. Using manufacturer's data as a starting point, the relative dielectric constant and attenuation constant of the line sections were taken into account, A more accurate value of the relative dielectric constant was later derived from time domain plot information (round-trip time delay) and from knowledge of the physical length of the cable minus

its connectors, Refinement of the attenuation constant value was later achieved through the use of **pre-environmental** cable loss data and a technique [1] that involved removal of connector mismatch effects.

The next step was to cascade the individual networks and calculate the overall S-parameters of the cable. If a program for cascading two-port networks is not available, one can proceed as follows, Begin by calculating the S-parameters of a basic network consisting of a single shunt discontinuity and a length of **lossy** line (see Appendix A for equations). Then cascade two basic networks, using cascading equations given in [2], and calculate the overall S-parameters of the resulting equivalent single two-port network, Next cascade this equivalent two-port network with the next basic network and again calculate the overall S-parameters of the **new equivalent** two-port network. Repeat the process until all basic networks of the cable model are cascaded.

After deriving the overall S-parameters, the attenuation [3] of the cable was calculated at each frequency from

$$A = 10 \log_{10} |S_{21}| \quad (1)$$

where S_{21} is the overall transmission coefficient of the cascaded basic networks of the cable. This procedure led to the desired theoretical data set, Return loss data sets were obtained by converting S_{11} and S_{22} data into decibels. For this article, these other data sets were not actually used in the modeling process, but were used later for comparison purposes.

The final step in the modeling procedure was to compare the theoretical and experimental cable attenuation data sets, If the agreement between theoretical and experimental data was unsatisfactory, then the shunt susceptance and length values were adjusted and the S-parameters at

each frequency were recalculated to derive a new theoretical data set. The process was repeated until a specified criterion for goodness of fit between theoretical and experimental values was met,

B. COMPUTER-AIDED PROCEDURE

1. Nonlinear Squares Fit Program

It is common practice to best-fit polynomial curves to experimental data because a polynomial curve-fitting process is easy to perform and useful for displaying trends. In addition, intermediate values and standard deviations are easy to calculate. What is not generally known, is that if a physical phenomenon associated with the experimental data can be modeled mathematically (no matter how involved and complex), then the modeled-theoretical data can be best fitted to experimental data through the use of an NLSF program, Most NLSF programs are easy to use. Variance, correlation coefficients, and standard deviations can also be easily computed from the residuals of the nonlinear curve-fitting process.

A linear model is defined here as one whose coefficients a_i can be expressed explicitly in the form

$$y(x) = a_0 + a_1 f_1(x) + a_2 f_2(x) + \dots + a_i f_i(x) + \dots + a_n f_n(x) \quad (2)$$

Polynomials are a subset of the general linear form given by Eq. (2). A nonlinear model differs from the above in that the coefficients or parameters to be solved for (best fitted) can be expressed within any of the expressions for $f_i(x)$ or in almost any mathematical form. As long as the program steps can be written to calculate values of $y(x)$ for input values of x , then a nonlinear least-squares fit can be performed to solve for the unknown parameters.

To use most NLSF programs, the user must provide (1) the experimental data set, (2) the subroutine program to calculate the theoretical values for the mathematical model, and (3) estimates of the nominal or starting values of the parameters to be best-fitted. More advanced NLSF programs allow bounds to be specified so that the best-fitted parameter values will stay within physical realizable limits. From the provided input data and subroutines, the NLSF program finds the parameter values that give the best fit (using a least-squares convergence criterion) between theoretical and experimental values.

2. Applications to Cable Problems

The particular NLSF program [4] employed to obtain improved models described in this article is public domain and can be run on a personal computer. This program allows bounds to be specified on the parameters to be best fitted so that the values stay within physical realizable limits.

The procedure, for developing cable models with the aid of an NSFL program follows that of the general procedure described in Section 11A. The parameters, to be adjusted by the NSFL program, were specified to be (1) the discontinuity magnitudes (in terms of shunt susceptance or capacitance values) and (2) the line lengths separating the discontinuities. Even though the distances between the **discontinuities** were allowed to be adjusted within specified bounds, the program was written so that the resulting overall length of the cable for the model had to be equal to the actual physical length of the cable.

111. RESULTS

A. EARLY MODELS

The Galileo cable modeling work was initially done without the benefit of an NLSF program because a suitable program, that allowed bounds to be specified on the parameters to be adjusted, was not yet available at JPL. The early work had to be performed on a crash program basis to explain the unusual characteristics seen on the Galileo antenna cable after the environmental testing. A lack of an explanation would have caused an indefinite delay in the shipment of Galileo to Cape Canaveral. The results of this early work are described below.

From the time domain plots described in Section II, it was determined that a total of four distinct **discontinuities** existed near cable clamp and connection regions [5]. When the unaltered values (extracted directly from return-loss time domain plots) were used in Model 1, the agreement between theoretical and experimental data was poor. The parameters for the subsequently developed Model 2 were almost the same as those of Model 1, except that the line lengths between **discontinuities** were intentionally adjusted to cause **all** the individual reflection coefficients to add up in phase at the cable input port at 2310 MHz. As can be seen in Fig. 1, the agreement for Model 2 was reasonable at mid-band, but. was poor at frequencies toward the band
e d g e s .

During this early work, it was surmised that if one more discontinuity (towards the end of the cable) were added to Model 2, then better agreement between theory and experiment could be obtained over more of the frequency band, However, further attempts to add one more discontinuity and then readjust all the line lengths and **susceptance** magnitudes (by trial and error) for a good fit proved to be an excessively **time-consuming** and fruitless effort. It was clear that some type of least-squares fitting program was required to help develop an improved model.

Although not perfect, Model 2 provided a satisfactory explanation of the cause of the unusual behavior, and a decision was made not to replace this antenna cable. The Galileo spacecraft was shipped to Cape Canaveral on schedule, and the need for improved models vanished.

'B. IMPROVED MODELS

When an advanced type of NLSF program (described in Section IIB) became available at JPL, the modeling work was resumed and new models were subsequently developed. The work was resumed primarily in the interest of learning how to use NLSF programs for other JPL applications. However, since experimental data were already available, the Galileo cable problem provided the ideal test case.

After the development of Model 2, it was known that additional discontinuities in the cables existed near the connector interfaces. Examinations of detailed drawings of the connector regions revealed locations of potential discontinuities that were not taken into account in Model 2. Figure 2 shows potential discontinuities as being the back ends (or sharp edges) of the rigid Kynar sleeves, located about 2.9 in.¹ from the faces of the cable connectors. Bending of the cable at these points can cause crimps or make permanent deep creases on the outer diameter. Another type of potential discontinuity occurs at the connector regions (Fig. 3) where there are changes in diameter dimensions and dielectric materials within the coaxial transmission line. As shown in Fig. 3, the nominal inner and outer diameter of the coaxial transmission line are 0.090 and 0.241 in., respectively, and the relative dielectric constant was determined to be 1.34 [5].

¹The units are in inches rather than in centimeters, because all original drawings and data were presented for cable dimensions in inches. To avoid confusion when referring back to earlier reports, the units of inches are retained in this article.

Two likely equivalent circuits for the cable **discontinuities** are (1) shunt capacitances whose susceptance values are functions of frequencies and (2) capacitive shunt susceptances whose values do not change over the frequency of interest. The following presents two improved models based on these two types of **discontinuities** and derived with the aid of the described NLSF program.

1. Model 3

Model 3 represents the cable **discontinuities** as constant shunt capacitances. The constant shunt capacitance might occur in practice when the reduced outer diameter of the cable is squashed over some physical length (e.g., the cable clamp width). For this type of discontinuity, the magnitude of S_{11} of the individual discontinuity changes with frequency (see Appendix A). For this model with nominal values, the final best-fit parameters determined by the NLSF program are shown in Fig. 4. Note that the locations of **discontinuities** of the model occur very close to actual locations of the cable clamps, the edges of the Kynar sleeve, and the connector **discontinuities**.

Figure 5 shows the comparison between theoretical and measured insertion losses. It can be seen that the agreement is significantly better than that of the Model 2 fitted curve shown in Fig. 1. To obtain this excellent fit, it was necessary to use accurate values of cable attenuation due to **line losses** between the shunt **discontinuities** [1]. Although Model 3 appears to be an excellent model, it was found to be incorrect, As maybe seen in Fig. 6, when all the **discontinuities** are removed except the two outer connector **discontinuities**, the agreement between theory and the pre-environmental test data becomes progressively worse at the higher frequencies.

2, Model 4

Model 4 is based upon representing the **discontinuities** as constant susceptance values over the frequency range of interest (see Appendix A). This type of discontinuity could be a deep crease, or crimp, on the outer diameter of the cable. Such a discontinuity in practice can be created by bending the cable against the edge of a cable clamp or the edge of a Kynar sleeve. This type of discontinuity can be represented as two shunt capacitances separated by a short distance (less than 0.005 wavelength, or a single shunt **susceptance**, as discussed in Appendix B).

The overall equivalent circuit and locations of the **discontinuities** along the cable are shown in Fig. 7. Model 4 is the result of best fitting 15 parameters (seven **discontinuities** and eight line lengths) by using 101 frequency points for a **frequency** range of 1.7 to 2.85 GHz. As with Model 3, the line losses between **discontinuities** for Model 4 were properly accounted for at each frequency. When the NLSF program and cable model subroutines were run on an IBM-XT type personal computer, it took about 5 hours to obtain best-fit parameters for this model. Even though time consuming, the cost to run the program was negligible and speed of computations was not a critical factor. Once the **desired** parameters and bounds were specified, the entire best-fit process was performed automatically.

The Model 4 discontinuity locations, shown in Fig. 7, correspond very closely to the actual locations of cable clamps, the edges of the Kynar sleeve, and internal discontinuities of the connectors. The locations of the modeled **discontinuities** are estimated to be within ± 0.5 in. of the actual cable discontinuities.

It can be seen in Fig. 8 that the theoretical values for this model agree well (within ± 0.02 dB) with experimental data. Good agreement between theoretical and experimental return losses was also obtained, as can be seen in Figs. 9 and 10. It is generally known that for a transmission line

having two small discontinuities separated by a large distance, the theoretical insertion loss' characteristics as a function of frequency will be sinusoidal [6]. Figure 11 shows that when all internal discontinuities except the two outer discontinuities were removed, the agreement between the model and pre-environmental test data was excellent.

To ensure that Model 4 is, in all respects, the correct model of the cable, the phases as well as the magnitudes of S_{21} were considered. However, attempts to fit both magnitudes and phases to experimental data were unsuccessful. Also, the attempt to do similar least-squares fitting to the S_{11} and S_{22} experimental data proved unsuccessful. It was later revealed that special adapters had been used to measure the reflection coefficients S_{11} and S_{22} . When the effects of the adapters were gated out,² the measurement planes might not have been properly referred back to the connector interface planes of the cable [7]. It is difficult to best fit phase data if the measurement and model reference planes do not coincide.

Due to the difficulty of obtaining a good fit between the theory and the model, based on both S-parameter amplitude and phase data, another method was used to verify the model. This method compared experimental and theoretical time domain plots. Time domain plots require both magnitude and phase information over a wide frequency range. Figures 12–14 show time domain plots for S_{21} , S_{11} , and S_{22} data, respectively. Good agreement was obtained for S_{21} , but for the S_{11} and S_{22} time domain plots, the reference planes had to be shifted by an amount approximately equal to the lengths of the special adapters used in the measurement. The necessity to shift reference planes for S_{11} and S_{22} is consistent with the possibility that the measurement plane might not have been correctly referenced back to the cable connector interface planes. Despite the described difficulties with the reference plane problem associated with the S_{11} and S_{22} time domain plots, good agreement was obtained for the S_{21} time domain plot. One can conclude from

²See *Hewlett Packard 8510B Operating Manual* for a discussion of gating techniques for the purposes of removing external discontinuity effects from the measured S-parameter data.

the data presented that Model 4 is an excellent representation of the Galileo S-band cable after the environmental tests.

For follow-on work, a Model 5 could be developed with **discontinuities** inside the cable being represented by constant shunt capacitances and the connectors represented as constant shunt **susceptances**. It is expected that such a model would give results that are similar to those for Model 4.

IV. CONCLUSIONS

With the aid of the NLSF program, a **model** has been found that gives excellent agreement **between** theory and experiment for the Galileo spacecraft S-band antenna cable. The final model now has seven **discontinuities** (including connectors) instead of four obtained for Models 1 and 2.

The sharp edges of the cable clamps and the Kynar sleeves are the probable causes of the **discontinuities** on the outer diameter of the cable. The cable clamps should be **redesigned** so that crimping or creasing will not occur when the cable is bent against the clamps. It was shown in [5] that a 0.02-in. reduction in outer diameter of the Galileo cable could produce **discontinuities** of the magnitudes presented in the models studied. For antenna cables to be used on spacecraft in the “future, the edges of the currently rigid sleeves should also be redesigned and be made flexible. ,

The method presented here was demonstrated for a coaxial cable, but the technique can be extended to the modeling of **discontinuities** in other types of transmission lines, such as rectangular and circular **waveguides**.

ACKNOWLEDGMENTS .

Dr. C. Lawson, at that time Supervisor of the Applied Mathematics Group at JPL, supplied the public domain NLSF software and assisted with the coding procedures. Scott Stewart, a contractor from PRC in Pasadena, California, programmed the HP 85 10B Network Analyzer computer to read theoretical S-parameter data into data files for the purpose of generating theoretical time domain plots. Technical discussions with Kent Kellogg and Phil Stanton of JPL were helpful. The measured S-parameter data were provided by the Spacecraft Antennas Group at JPL.

Appendix A

S-Parameters of a Basic Network

The basic network used in the modeling work is shown in Fig. A- 1. The elements of the network are a capacitive shunt susceptance followed by a length of lossy transmission line. The S-parameters for this network are

$$[s] = \frac{1}{2 + jb} \begin{bmatrix} -jb & 2e^{-\gamma\ell} \\ 2e^{-\gamma\ell} & -jbe^{-2\gamma\ell} \end{bmatrix} \quad (\text{A- 1})$$

where b is the normalized shunt susceptance, γ is the complex propagation constant, and ℓ is the line length.

For the *Constant Capacitance Model*

$$b = 2\pi f C Z_0 \quad (\text{A-2})$$

where f is the frequency in hertz, C is the capacitance in farads, and Z_0 is the transmission line characteristic impedance in ohms.

For the *Constant Shunt Susceptance Model*, b is a constant, The nominal value of b for both models can be obtained from experimental return loss–time domain plots by using the relationship

$$b = \frac{2|S_{11}|}{\sqrt{1 - |S_{11}|^2}} \quad (\text{A-3})$$

$$|S_{11}| = 10^{-(RL_1/20 - A_{dB}/10)} \quad (\text{A-4})$$

where RL_1 is the positive decibel return loss value measured at port 1 and A_{dB} is the positive decibel value for the transmission line loss between the discontinuity and port 1,

Appendix B

Equivalent Circuits of a Cable With a Reduced Outer Diameter Section

The equivalent circuits of the section of coaxial transmission line with a reduced outer diameter over length ℓ are shown in Fig. B-1. The characteristic impedance of the nominal and reduced sections Z_{01} and Z_{02} , respectively, are

$$Z_{01} = \frac{60}{\sqrt{\epsilon'_1}} \ln \left(\frac{D_{O1}}{D_{I1}} \right) \quad (\text{B-1})$$

$$Z_{02} = \frac{60}{\sqrt{\epsilon'_2}} \ln \left(\frac{D_{O2}}{D_{I2}} \right) \quad (\text{B-2})$$

where D_{O1} and D_{O2} are the diameters of the outer conductors for the nominal and reduced sections, respectively. The symbols D_{I1} and D_{I2} are the diameters of the inner conductors for the nominal and reduced sections, respectively, and ϵ'_1 and ϵ'_2 are the relative dielectric constants of the media in the nominal and reduced sections, respectively.

Using the equations for the equivalent circuit shown in Fig. B-1 (b) given by Beatty [8] for a type of two-port standard, the value of $|S_{11}|$ can be calculated. That value is then used in Eq. (A-3) to compute an equivalent shunt susceptance corresponding to the equivalent circuit shown in Fig. B-2(c). If length ℓ is very short (<0.005 wavelength), representing a crimp or deep crease in the outer cable, then the discontinuity should be represented as a shunt capacitive susceptance b of constant value over the frequency range of interest. If the length ℓ is about 0.1-0.25 wavelength, or about equal to the width of a cable clamp, then the equivalent b shown in Fig. B-2(c) should be represented as a shunt susceptance with a capacitance of constant value. For other equivalent circuits, see [9]-[12].

REFERENCES

- [1] T. Y. Otoshi, "A Method for Modeling Discontinuities in a Microwave Coaxial Transmission Line," *Telecommunications and Data Acquisition Progress Report 42-110*, Jet Propulsion Laboratory, Pasadena California, pp. 128–150, August 15, 1992. This article contains additional details of the earlier modeling work. Applicable mismatch error and group delay equations are presented in the appendices.

- [2] D. M. Kerns and R. W. Beatty, *Basic Theory of Waveguides and Introductory Microwave Network Analysis*, New York: Pergamon, pp. 42-43, 1967.

- [3] R. W. Beatty, "Insertion Loss Concepts," *Proc. IRE*, vol. 41, no. 9, pp. 1112–1119, September 1953.

- [4] C. L. Lawson, "Nonlinear Least-Squares—Plain and Fancy," *Computing and Information Services News*, Jet Propulsion Laboratory, Pasadena, California, vol. 8, no. 4, pp. 6-7, April 1990.

- [5] T. Y. Otoshi, "Galileo Cable Study Report," JPL Interoffice Memorandum 3328-89-0108 (internal document), Jet Propulsion Laboratory, Pasadena, California, May 17, 1989.

- [6] R. W. Beatty and T. Y. Otoshi, "Effect of Discontinuities on the Group Delay of a Microwave Transmission Line," *IEEE Trans. Microwave Theory and Techniques*, vol. MTT-23, pp. 919–922, November 1975,

- [7] W. Folwell, personal communications, Spacecraft Telecommunications Equipment Group, Jet Propulsion Laboratory, Pasadena, California, 1990.

- [8] R. W. Beatty, "Calculated and Measured S_{11} , and S_{21} , and Group Delay for Simple Types of Coaxial and Rectangular Waveguide 2-Port Standards," *NBS Technical Note 657*, National Bureau of Standards, Boulder, Colorado, p. 18, December 1974.
- [9] N. Marcuvitz (Editor), *Waveguide Handbook*, (McGraw Hill Book Company, Inc., New York, New York, pp. 296,307, 1951.
- [10] J. R. Whinnery, H. W. Jamieson, and T. E. Robbins, "Coaxial-Line Discontinuities," *Proc. I.R.E.*, vol. 32, no. 11, pp. 695-709, November 1944.
- [11] P. J. Somlo, "The Calculation of Coaxial Line Step Capacitances," *IEEE Trans. on MTT*, vol. 15, no. 1, pp. 48-53, January 1967.
- [12] A. Jurkus, "Computation of Step Discontinuities in Coaxial Line," *IEEE Trans. on MTT*, vol. 20, no. 10, pp. 708-709, October 1972.

LIST OF FIGURES

Fig. 1. Comparison of experimental and Model 2 theoretical data,

Fig. 2. Galileo S-band cable outer dimension detail.

Fig. 3. Connector details,

Fig. 4. Model 3: (a) location of **discontinuities** relative to connectors and cable clamps and (b) equivalent circuit.

Fig. 5. Comparison of theoretical and measured insertion losses for Model 3, assuming shunt capacitance values that are constant over the frequency range of interest.

Fig. 6. Comparison of theoretical and measured insertion losses for Model 3 for the pre-environmental cable condition.

Fig. 7. Model 4: (a) location of **discontinuities** relative to connectors and cable clamps and (b) equivalent circuit.

Fig. 8. Comparison of theoretical and measured insertion losses for Model 4, assuming capacitive shunt **susceptance** values that are constant over the frequency range of interest.

Fig. 9. Comparison of theoretical and measured return losses for Model 4, as seen looking into port 1,

Fig. 10. Comparison of theoretical and measured return losses for Model 4, as seen looking into port 2.

Fig. 11. Comparison of theoretical and measured insertion losses for Model 4 for the pre-environmental cable condition.

Fig. 12. Comparison of theoretical and measured time domain responses on S_{21} data for Model 4.

Fig. 13. Comparison of theoretical and measured time domain responses based on S_{11} data for Model 4. The theoretical response curve had to be moved by the equivalent of 1.081 in. (0.212 nsec, round-trip) to the left in order to lineup the peaks of curves,

Fig. 14. Comparison of theoretical and measured time domain responses based on $|S_{22}|$ data for Model 4. The theoretical response curve had to be moved by the equivalent of 1.376 in. (0.270 nsec, round-trip) to the right in order to lineup the peaks of curves.

Fig. A-1. Basic network used in cable model,

Fig. B-1. Cable with a section of reduced outer diameter: (a) physical representation; (b) equivalent circuit with two capacitive shunt discontinuities separated by a line length of reduced section; and (c) equivalent circuit with a single shunt discontinuity and equivalent line lengths.

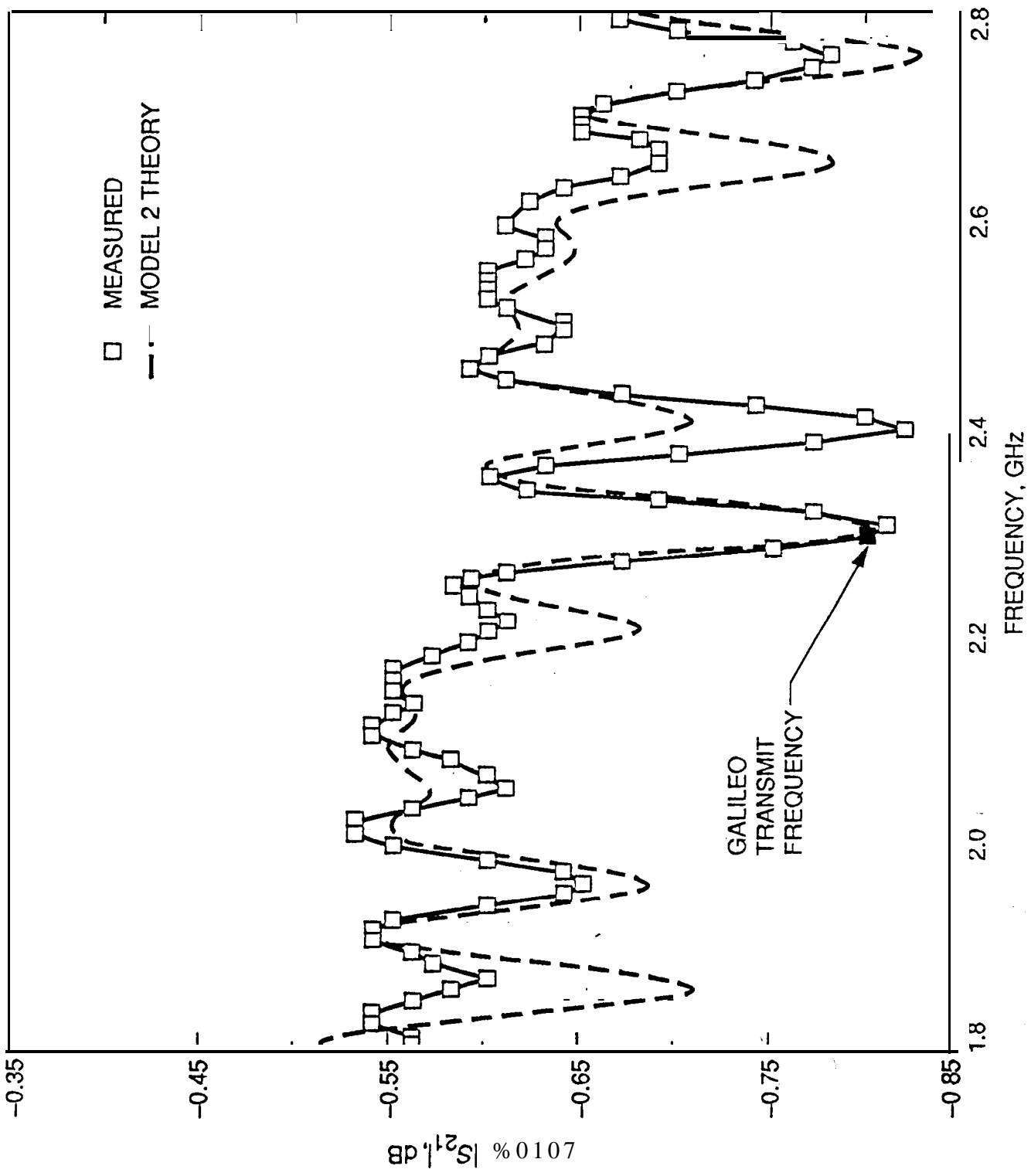


Fig. 1. Comparison of experimental and Model 2 theoretical data.

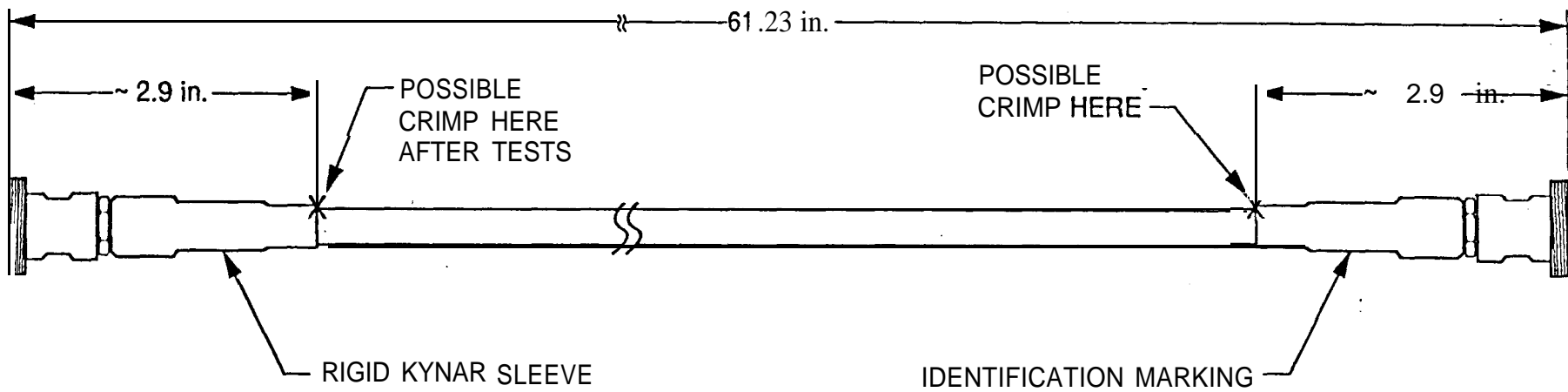


Fig. 2. Galileo S-band cable outer dimension detail.

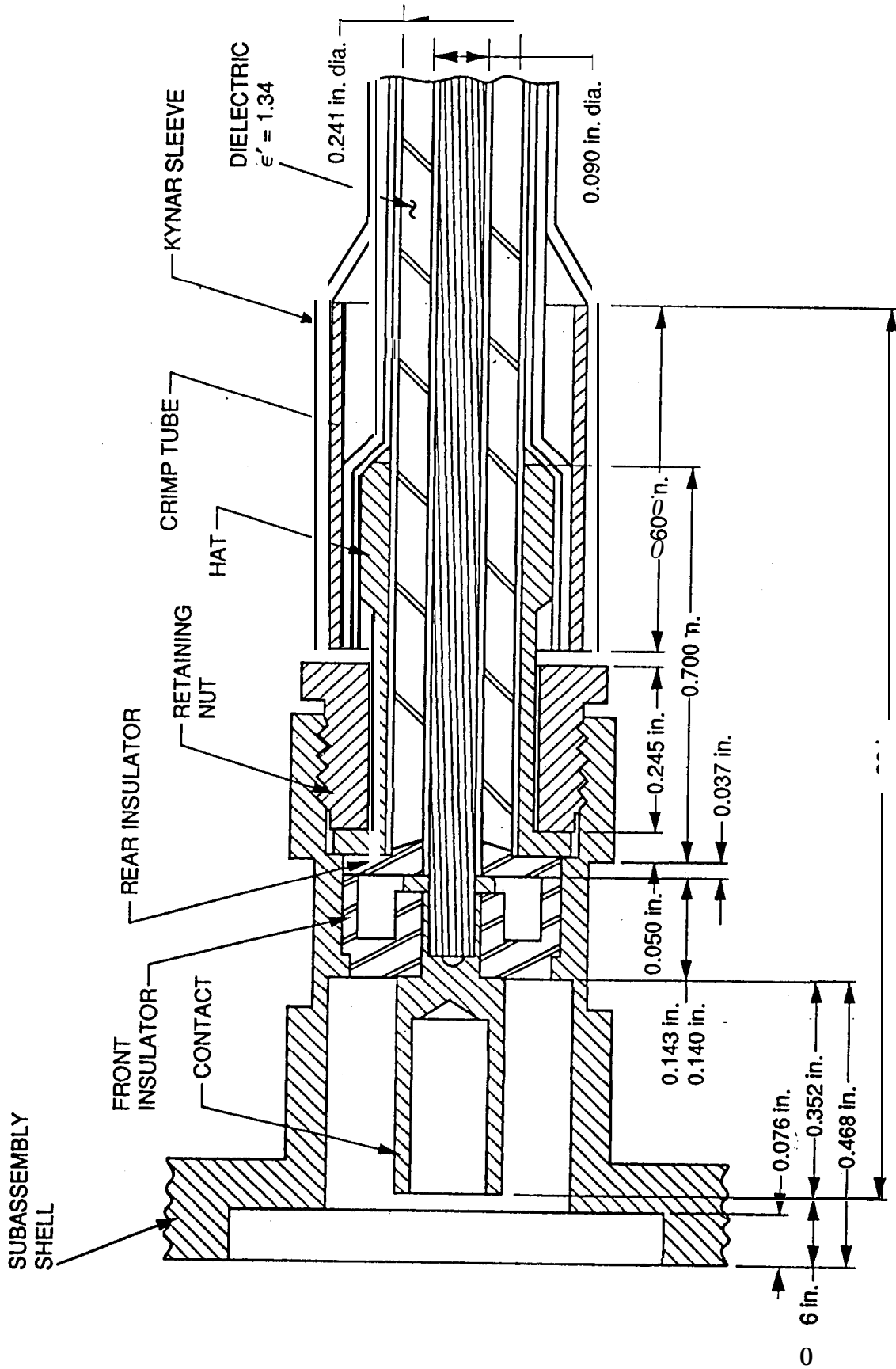


Fig. 3. Connector details.

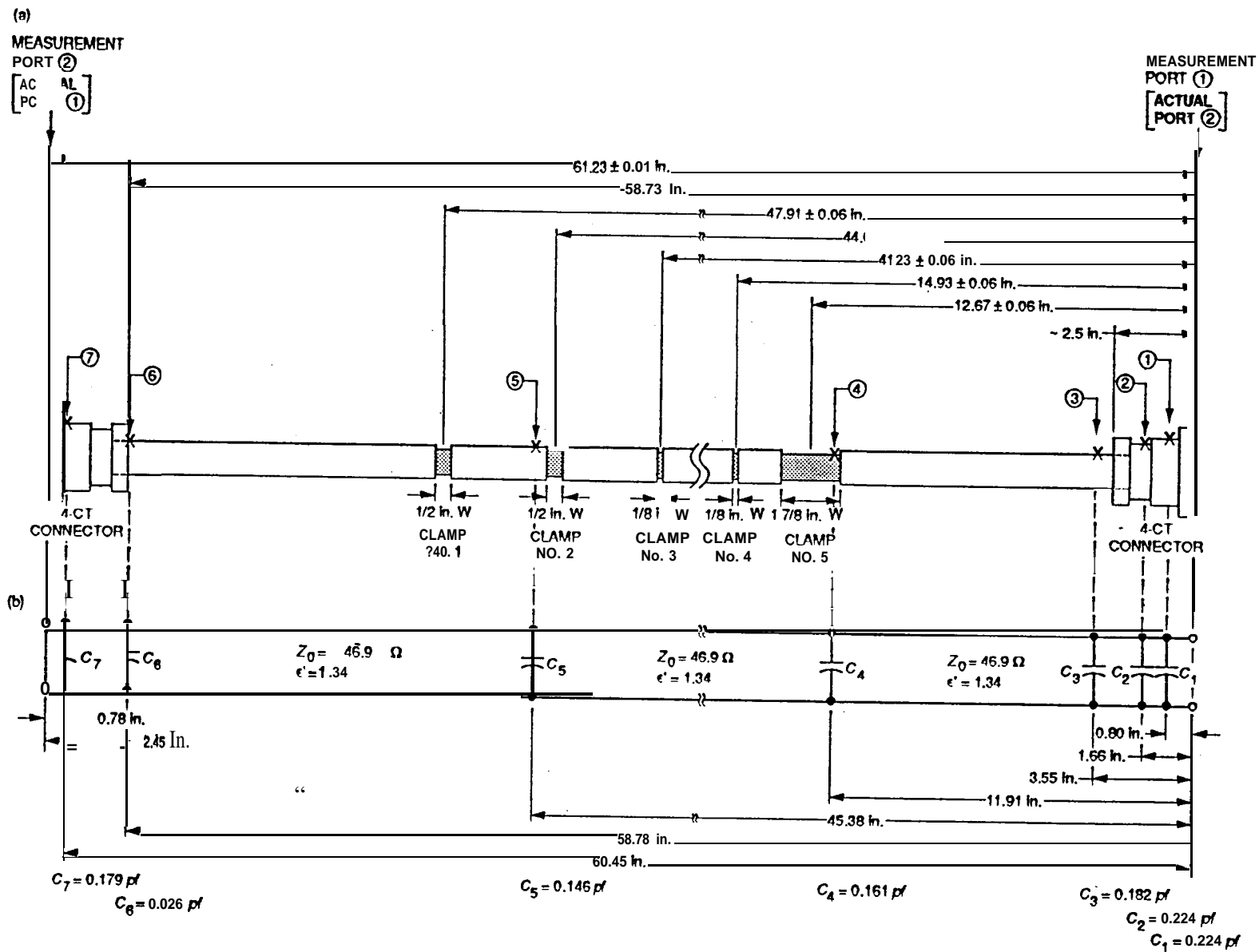


Fig. 4. Model 3: (a) location of discontinuities relative to connectors and cable clamps and (b) equivalent circuit.

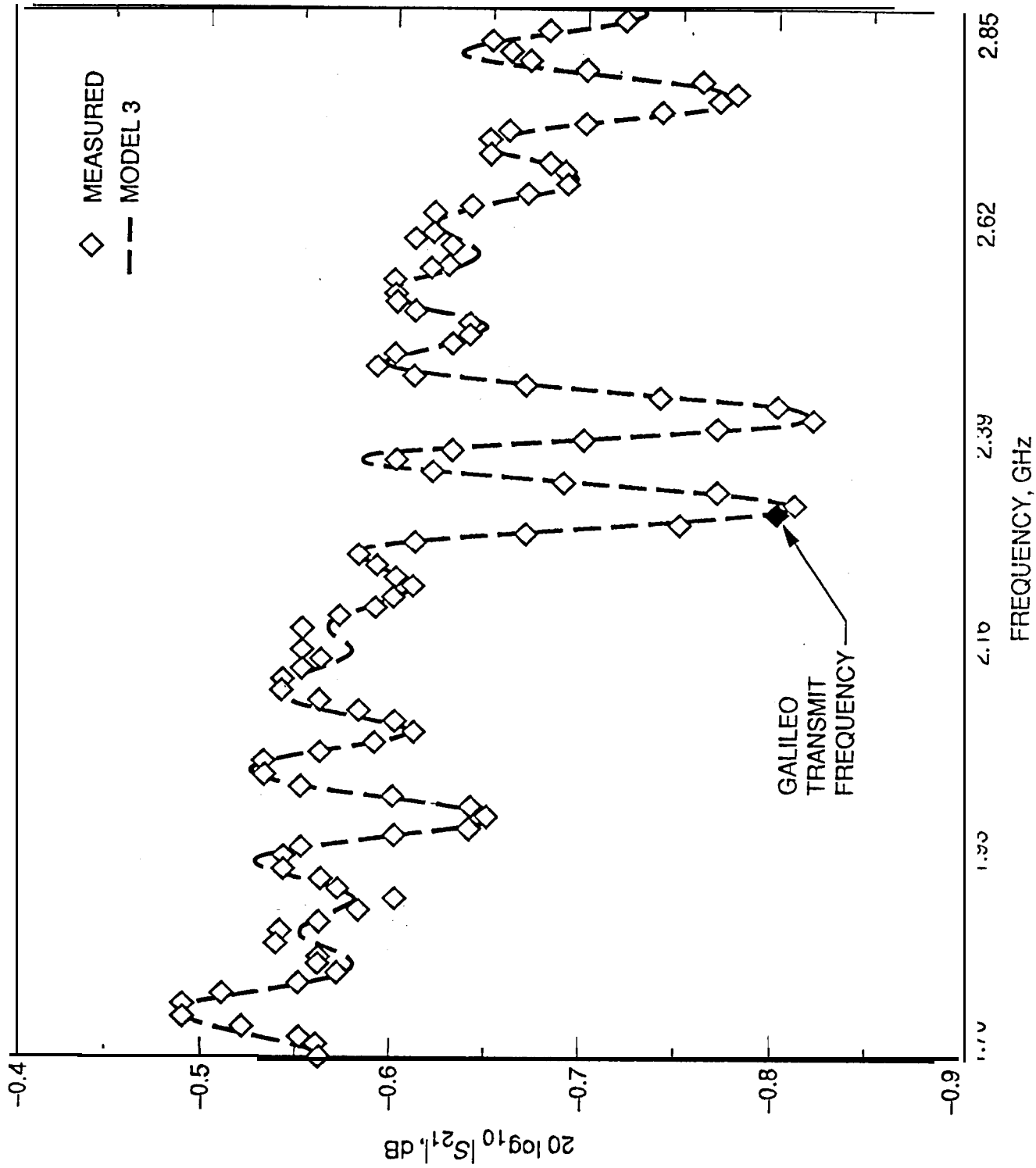


Fig. 5. Comparison of theoretical and measured insertion losses for Model 3, assuming shunt capacitance values that are constant over the frequency range of interest.

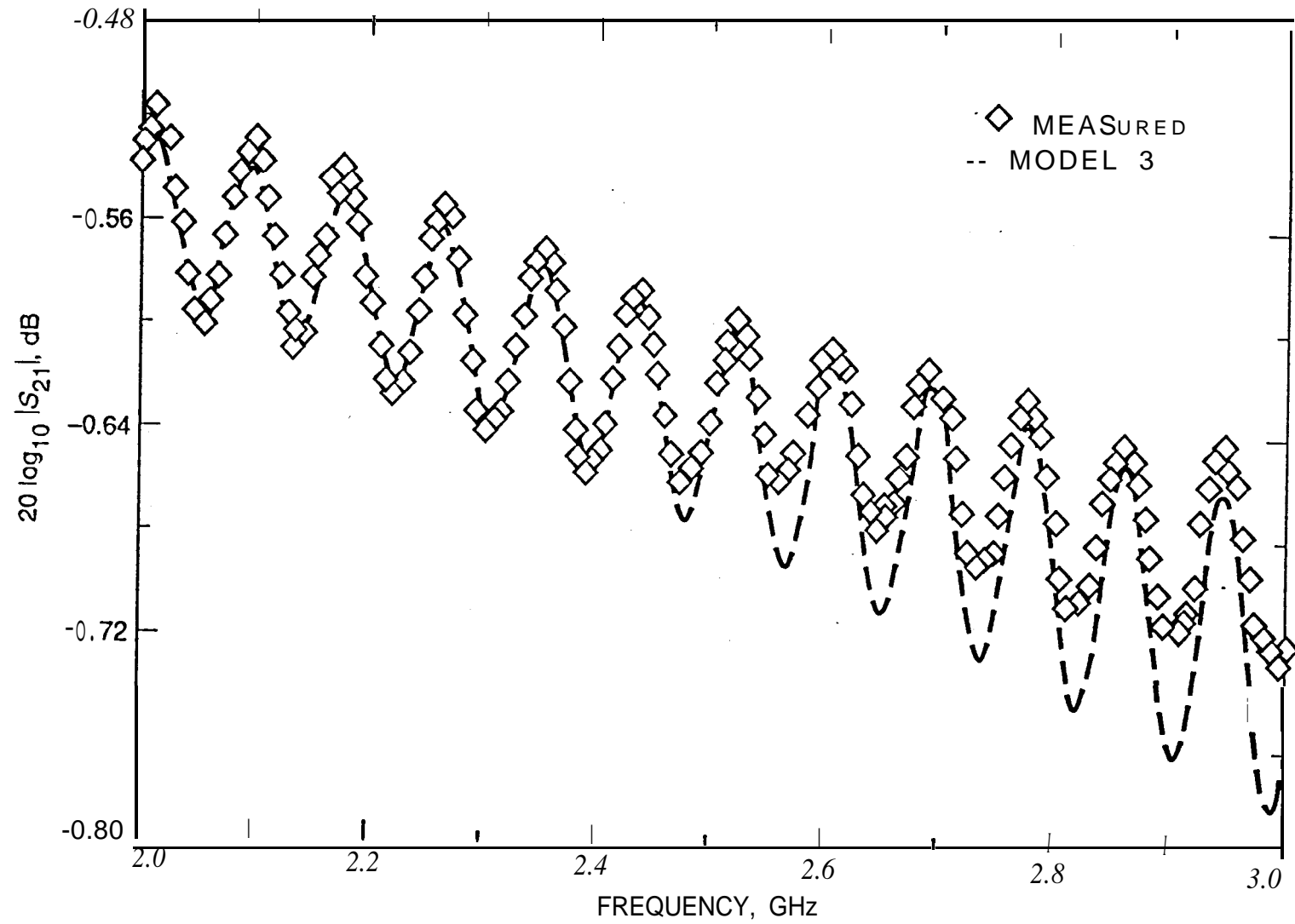


Fig. 6. Comparison of theoretical and measured insertion losses for Model 3 for the pre-environmental cable condition.

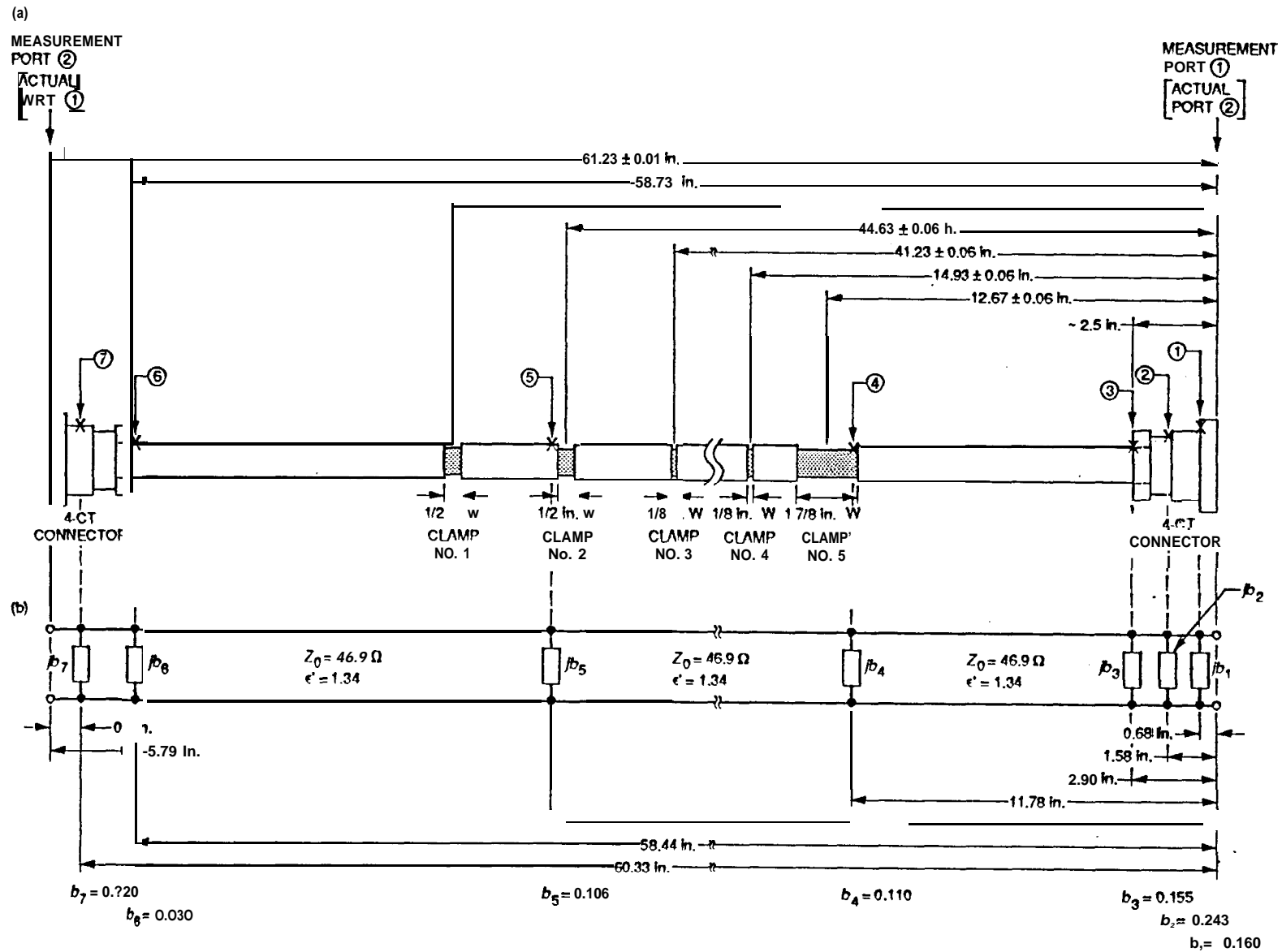


Fig. 7. Model 4: (a) location of discontinuities relative to connectors and cable clamps and (b) equivalent circuit.

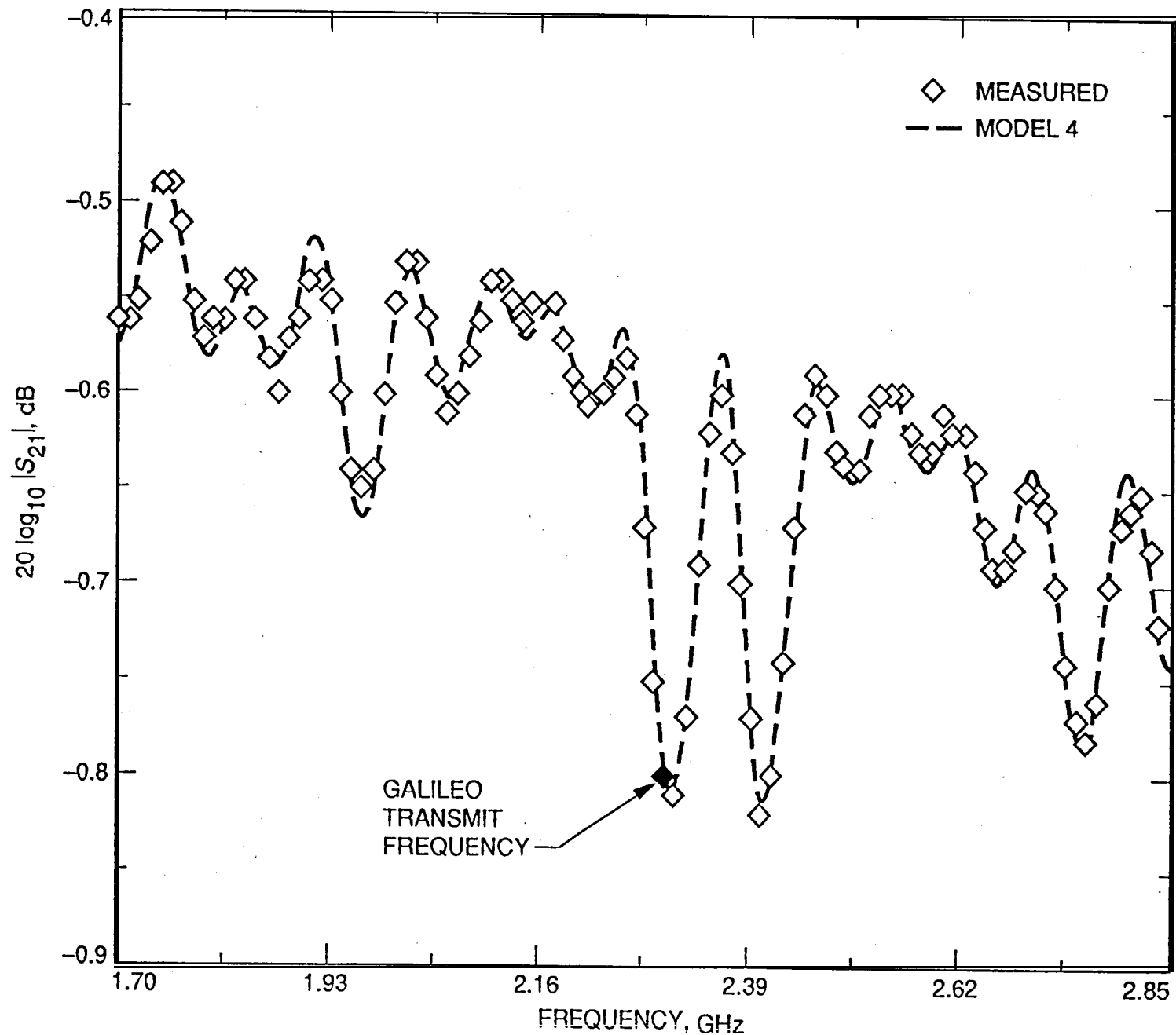


Fig. 8. Comparison of theoretical **and** measured insertion losses for Model 4, assuming capacitive shunt **susceptance** values that are constant over the frequency range of interest.

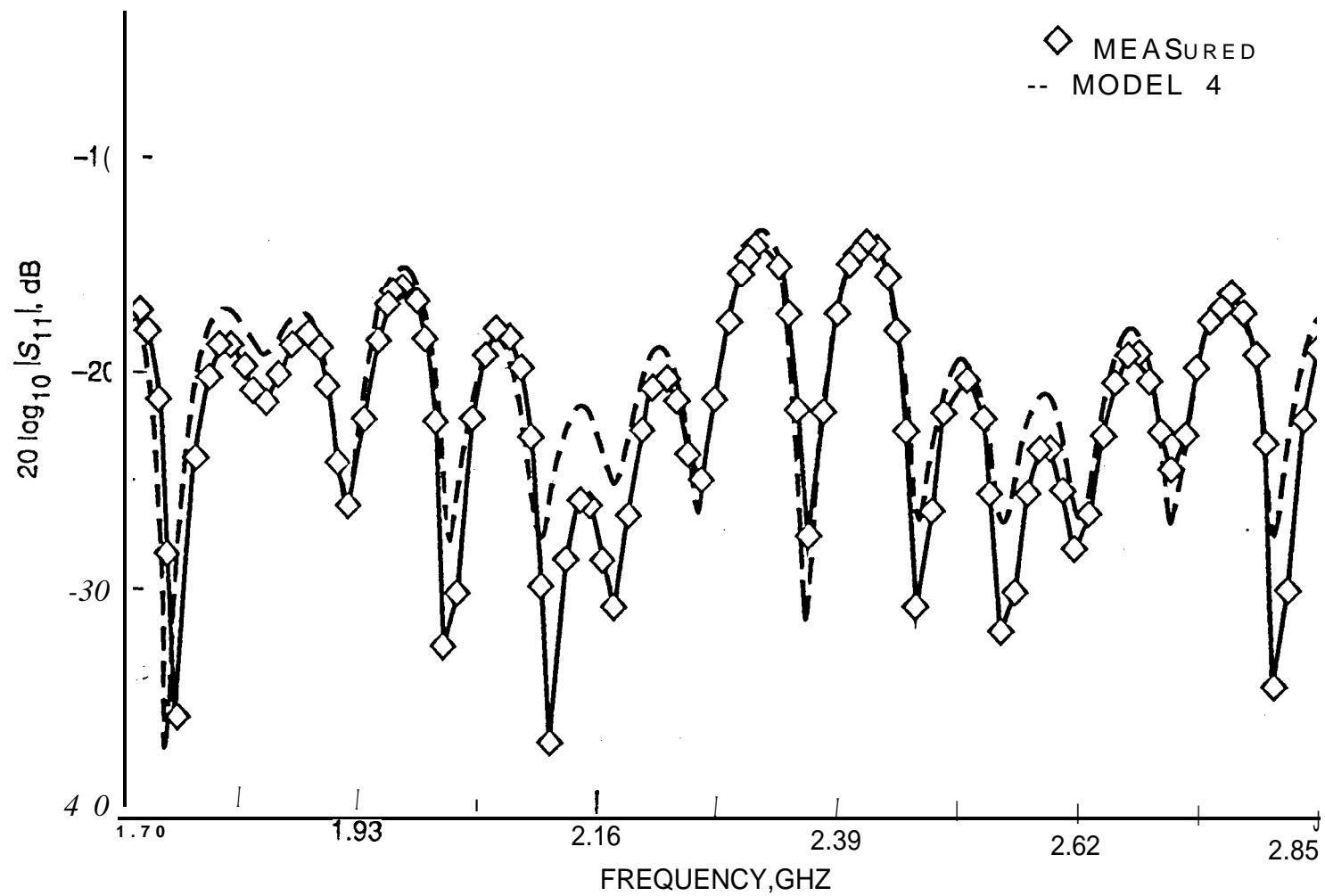


Fig. 9. Comparison of theoretical and measured return losses for Model 4, as seen looking into port 1.

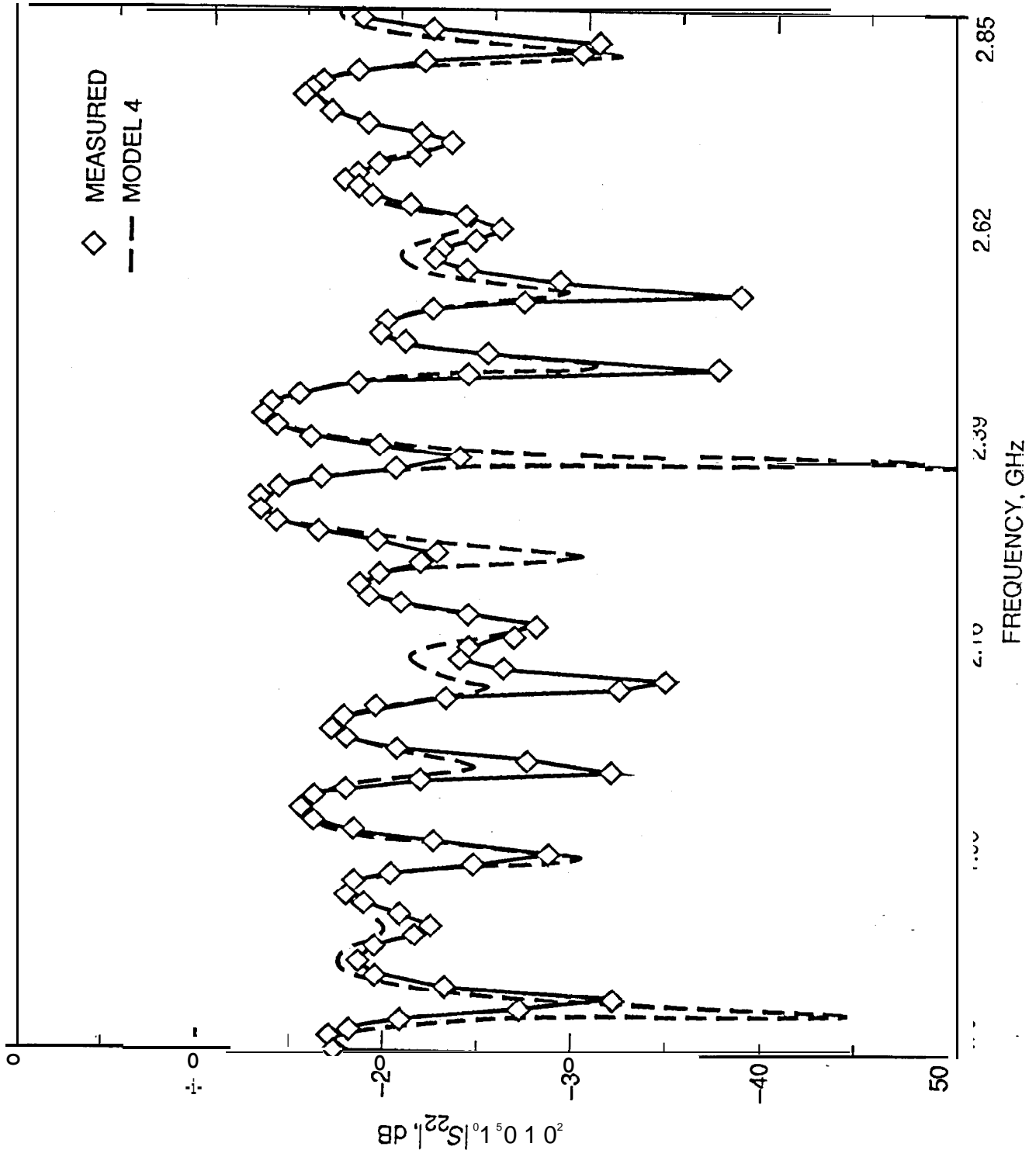


Fig. 10. Comparison of theoretical and measured return losses for Model 4, as seen looking into port 2.

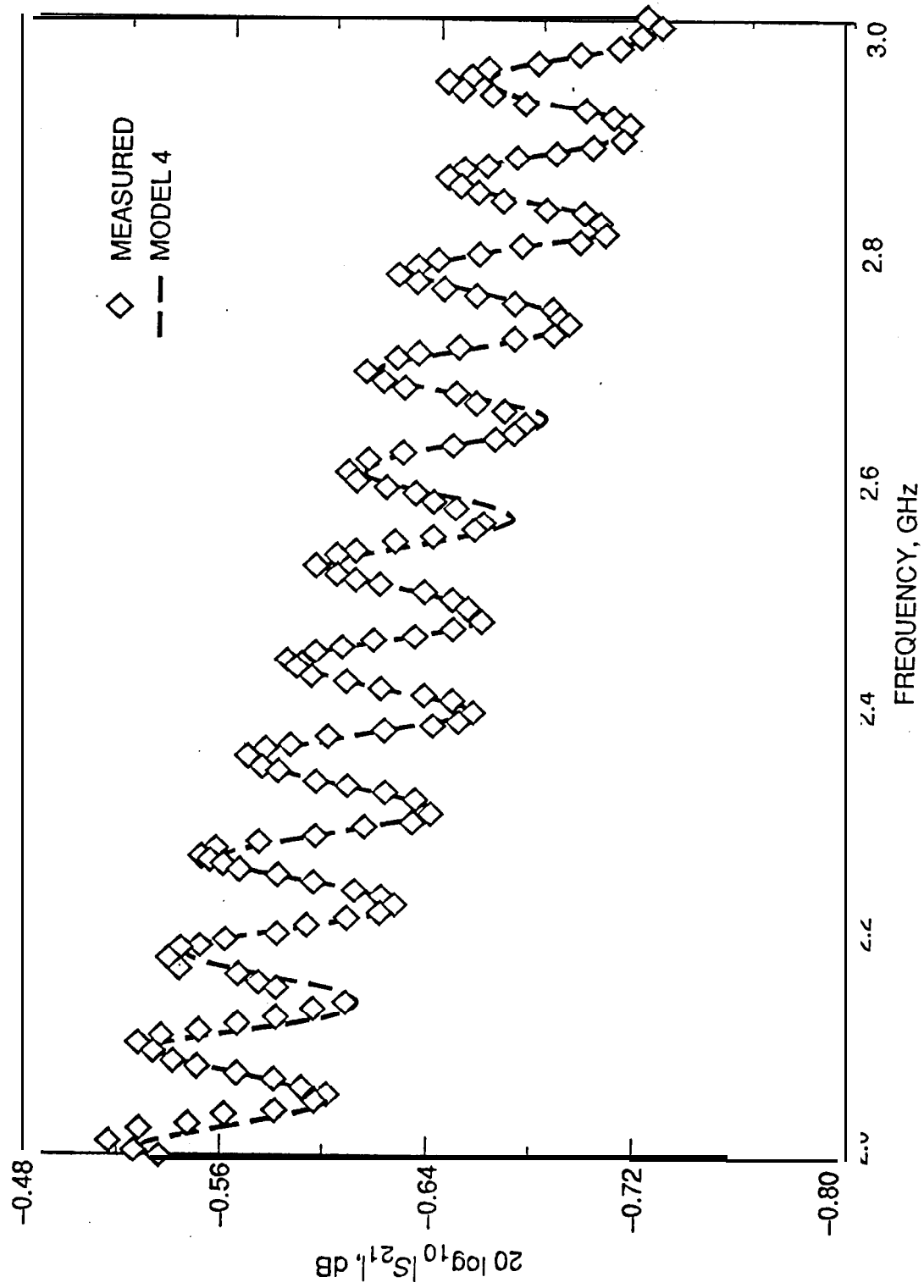


Fig. 11. Comparison of theoretical and measured insertion losses for Model 4 for the pre-environmental cable condition.

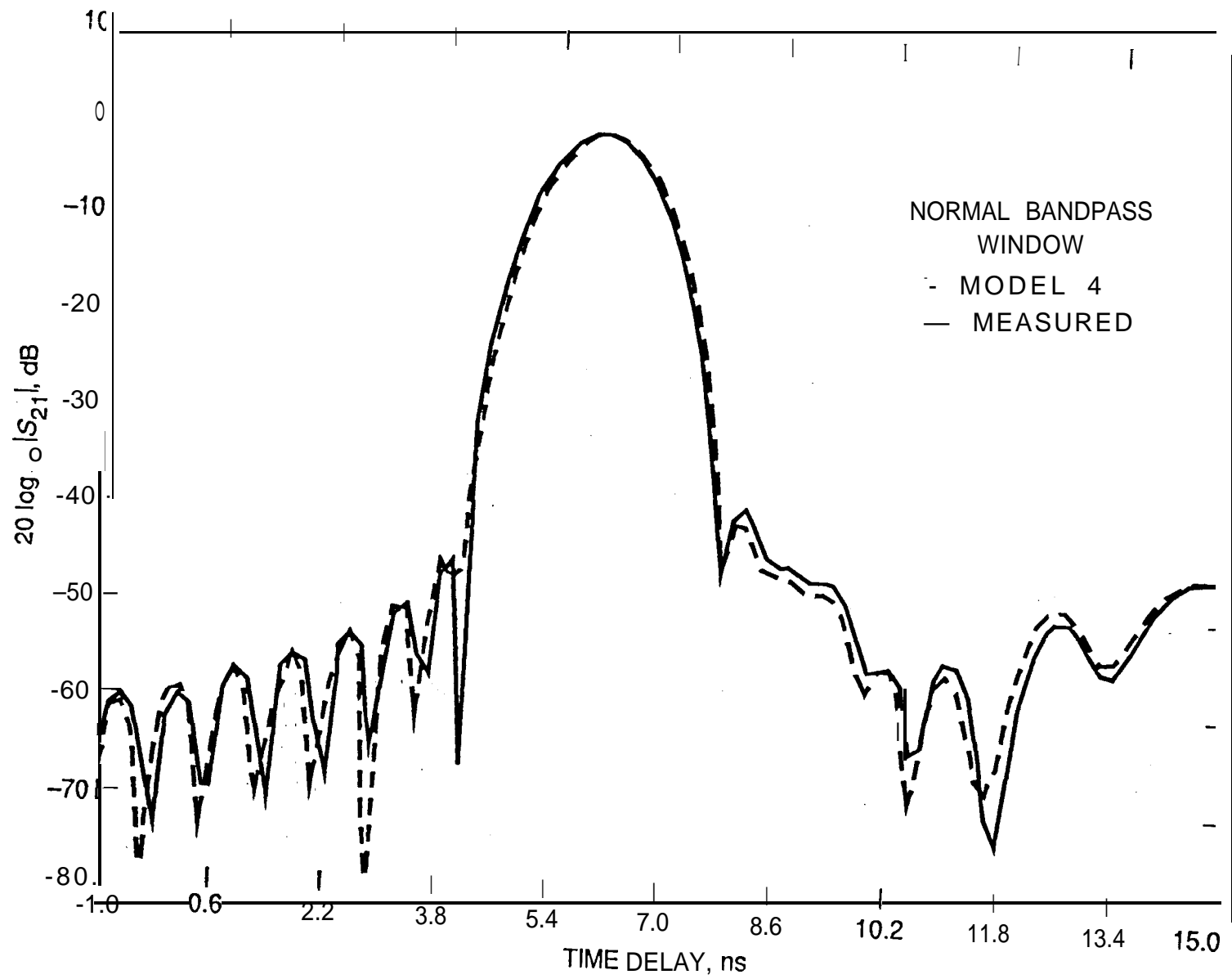


Fig.12. Comparison of theoretical and measured time domain responses on $|S_{21}|$ data for Model 4.

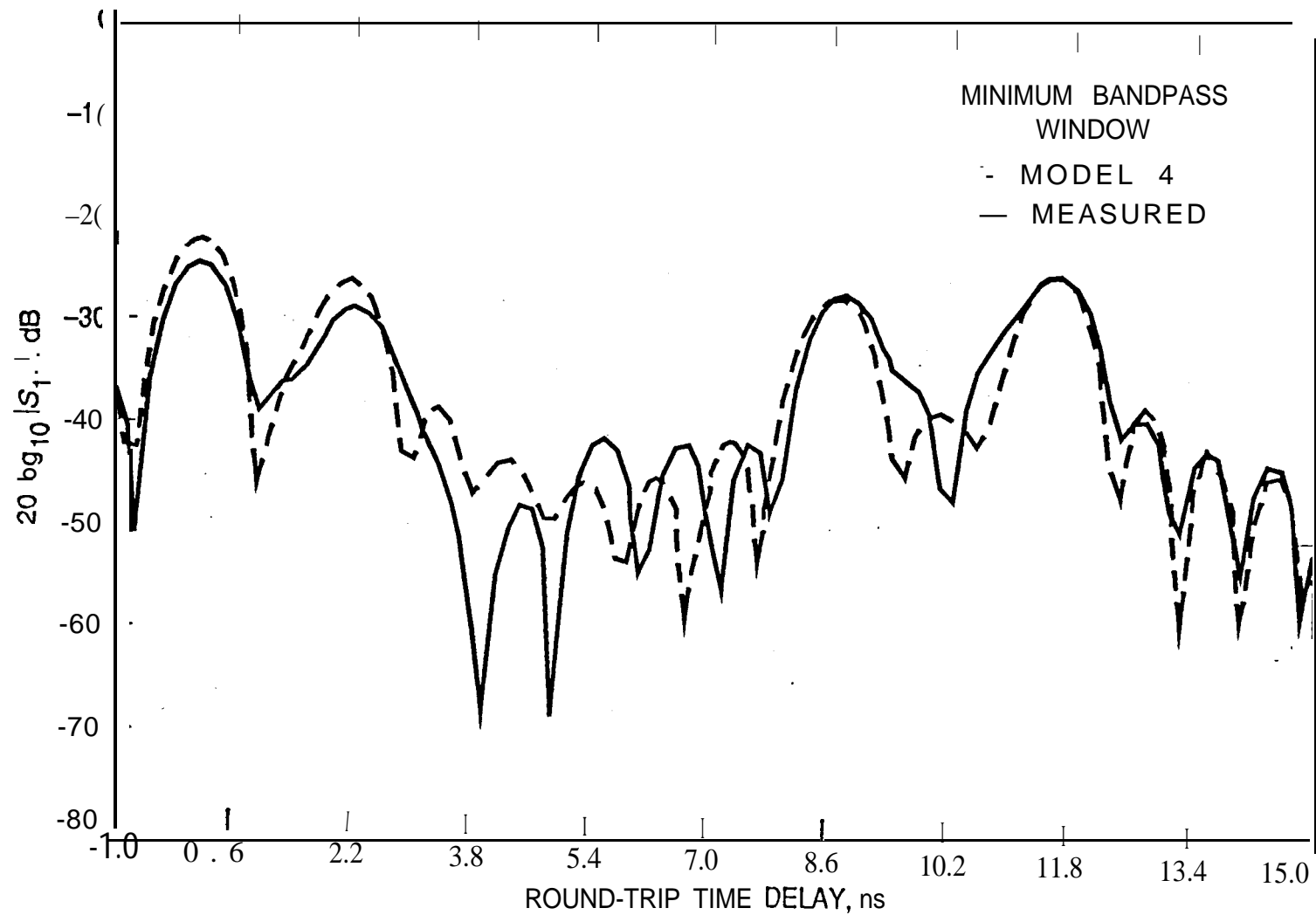


Fig. 13. Comparison of theoretical and measured time domain responses based on $|S_{11}|$ data for Model 4. The theoretical response curve had to be moved by the equivalent of 1.081 in. (0.212 nsec, round-trip) to the left in order to lineup the peaks of curves.

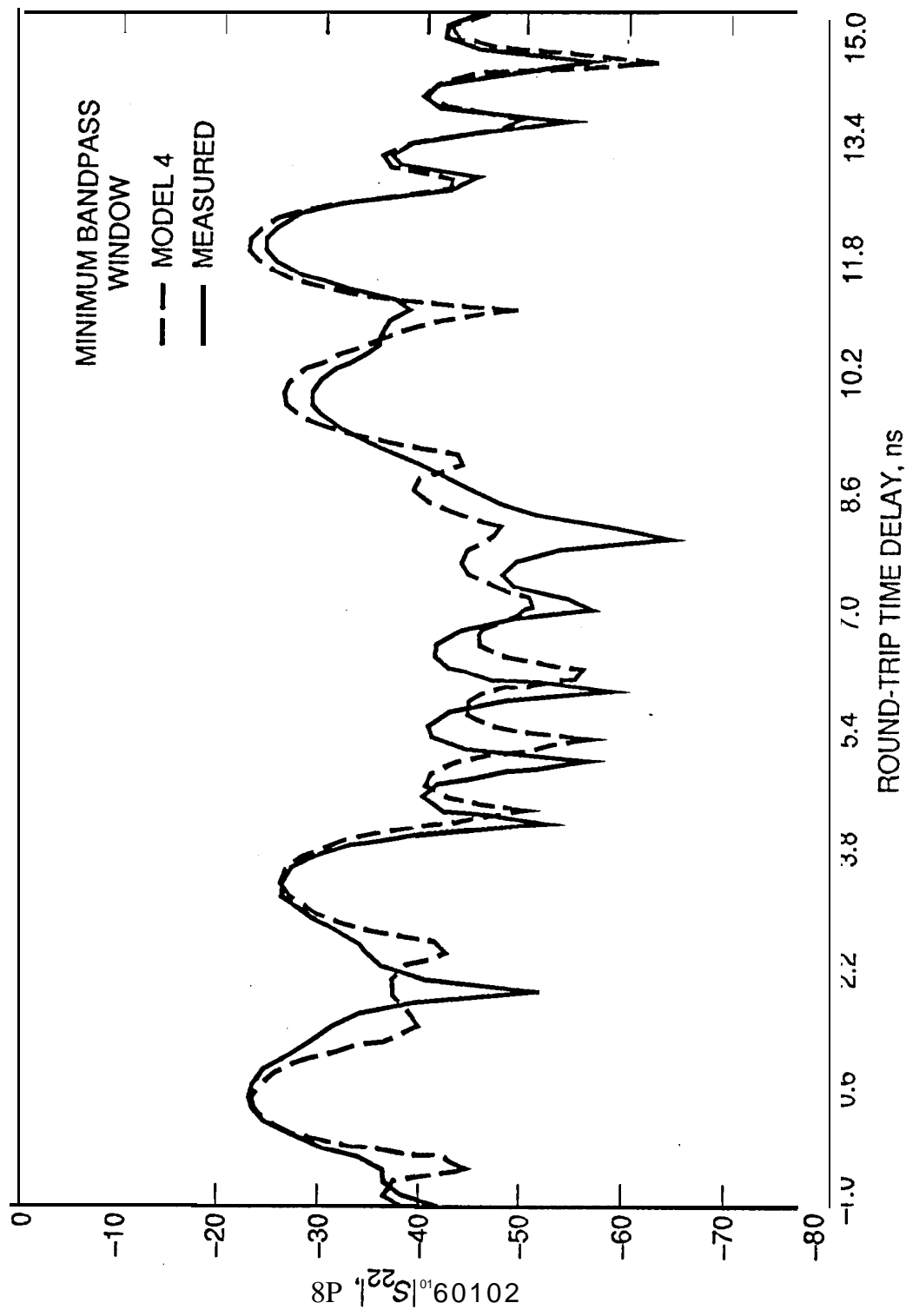


Fig. 14. Comparison of theoretical and measured time domain responses based on $|S_{22}|$ data for Model 4. The theoretical response curve had to be moved by the equivalent of 1.376 in. (0.270 nsec, round-trip) to the right in order to line up the peaks of curves.

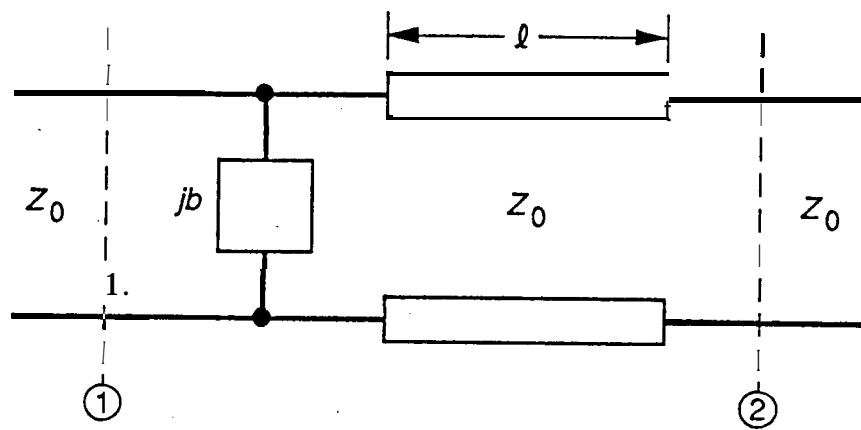


Fig. A-1. Basic network used in cable model.

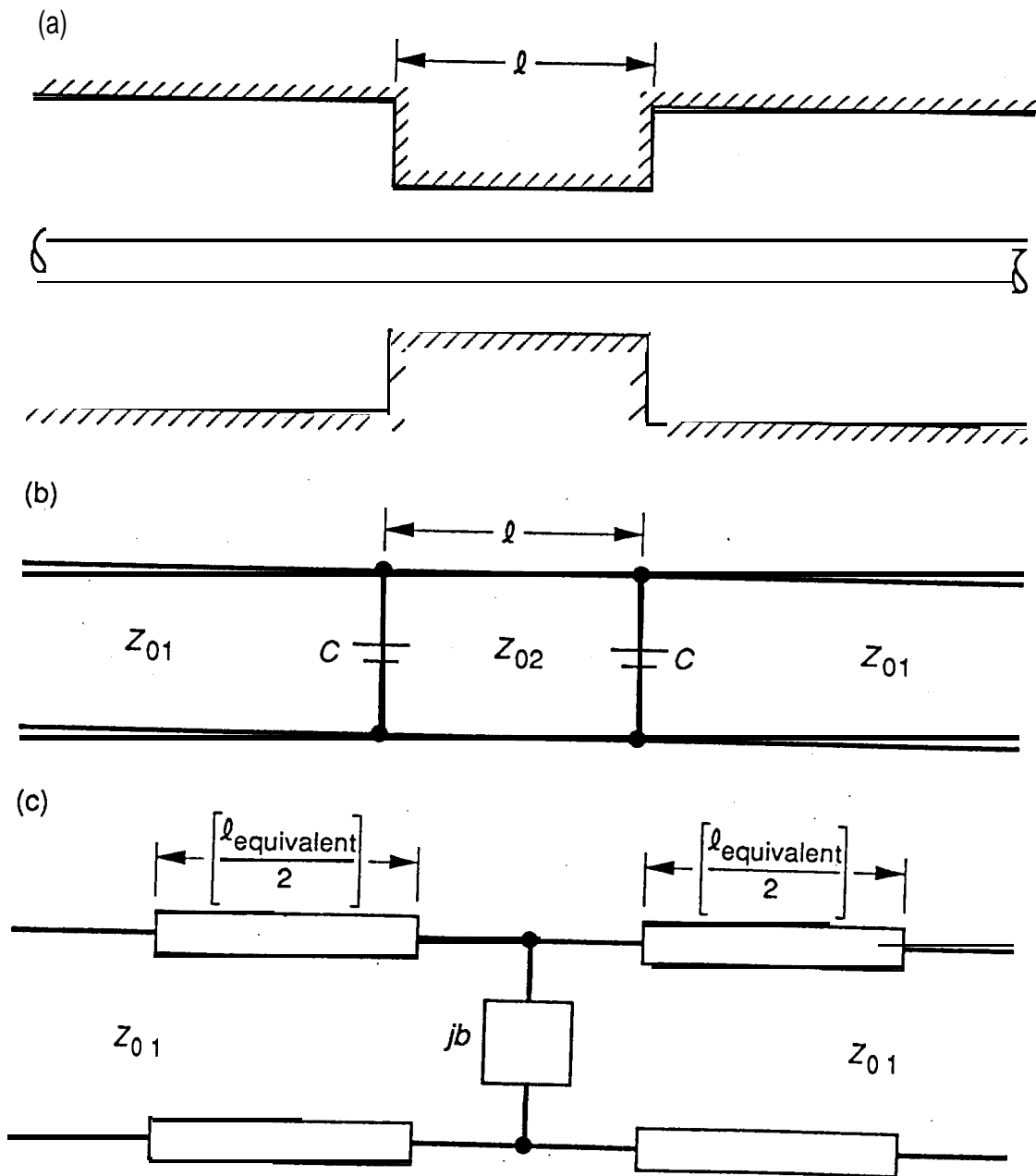


Fig. B-1. Cable with a section of reduced outer diameter: (a) physical representation; (b) equivalent circuit with two capacitive shunt **discontinuities** separated by a line length of reduced section; and (c) equivalent circuit with a single shunt discontinuity and equivalent line lengths.